Solid state resonant circuits and wireless electrical power propagation for mobile devices applications

Circuitos resonantes de estado sólido y propagación de energía eléctrica inalámbrica para aplicaciones de dispositivos móviles

Sergio Orendain-Castro [ID] [1], *Eduardo Murillo-Bracamontes* [ID] [2], *Oscar Edel Contreras-López*[2], *Alberto Hernández-Maldonado* [ID] [1]

[1]Facultad de Ciencias de la Ingeniería y Tecnología, Universidad Autónoma de Baja California, Unidad Valle de las Palmas, Tijuana, Baja California, México
[2]Centro de Nanociencias y Nanotecnología, Universidad Nacional Autónoma de México. Ensenada, Baja California, México

Corresponding author: Alberto Hernández Maldonado, Facultad de Ciencias de la Ingeniería y Tecnología, Universidad Autónoma de Baja California. Unidad Valle de las Palmas, Tijuana, Baja California, México. E-mail: hernandez.alberto@uabc.edu.mx, ORCID: 0000-0002-9768-4060.

Abstract. -. In this work, theoretical and experimental results of solid-state resonant circuits for the transmission and reception of wireless electrical energy, for applications in mobile devices are presented. Analytical expressions are found to calculate the voltage range as a function of the distance between the emitter and the load, as well as the current at the front end of an electromagnetic wave receiver. These expressions show the parameters to be varied to achieve a greater range in the transmission of wireless electrical energy. The transmitted voltage and current are measured by an electromagnetic wave receiver and compared with theoretical values, finding an excellent correspondence between the two.

Keywords: Wireless energy; Resonant circuits; Power propagation.

Resumen. - *E*n el presente trabajo se presentan resultados teóricos y experimentales de circuitos resonantes de estado sólido para la transmisión y recepción de energía eléctrica inalámbrica, para aplicaciones en dispositivos móviles. Se encuentran expresiones analíticas para calcular el alcance de voltaje en función de la distancia entre el emisor y la carga, así como la corriente en el extremo frontal de un receptor de ondas electromagnéticas. Estas expresiones muestran los parámetros a variar para lograr un mayor alcance en la transmisión de energía eléctrica inalámbrica. La tensión y la corriente transmitidas se miden mediante un receptor de ondas electromagnéticas y se comparan con valores teóricos, encontrando una excelente correspondencia entre ambos.

Palabras clave: Energía inalámbrica; Circuitos resonantes; Propagación de energía.

1.   Introducción

As is well known, the transmission of electrical energy is carried out through the use of electrical wiring, however, recent technological advances in the area of communications have motivated people to look for different ways of transmitting energy [1]. An example of this, are the cellular charging systems by magnetic induction [2, 3].

The transfer of electrical energy by magnetic induction through radio waves, was a problem initially raised by Nikola Tesla [4]. He worked on this problem, with the purpose of achieving a distribution of electricity wirelessly, over long distances.

We can classify wireless energy transfer systems into two types, inductive power transfer and magnetic resonance coupling and Near Field [5]. The inductive power transfer system uses a pair of coupled coils, at the transmitting side, an alternating current flow through the coil, generating a magnetic field, a second coil is used to receive the magnetic field and generate a current for energy storage. A magnetic resonant coupling system uses a pair of coupled coils with additional capacitance, which makes that the transmitter and the receiver have the same resonant frequency, which increases the efficiency and the transmission distance [6, 7].

Near Field Communication (NFC) is a technology that uses an inductive coupling technique oriented for mobile smart phone and operates at 13.56 MHz; it works via magnetic field induction and can transmit information in short distances up to a maximum rate of 424 Kbit per second. NFC systems are oriented to data exchange applications and usually used in mobile phones [8].

Some research from the Massachusetts Institute of Technology have worked in wireless power transfer because power cables reduce and limit the mobility of electronic devices. These investigations are based on magnetic induction techniques using new ring-shaped solenoid geometries. In these studies, it is possible to transfer electricity wirelessly, turning on a 60 Watts bulb, located 2 meters away, with an efficiency of 40% [9].

Some works have focused on the wireless transmission of electrical energy, using magnetically coupled aluminum and copper rings, achieving an efficiency of between 7% and 10% [10]. In these studies, the energy is used in the form of electromagnetic waves, using an emitter and receiver ring with resistive loads.

A related work demonstrated that the energy range of a wireless transmitter can be increased, by using a system of rings located at a distance of 0.4 meters between them, achieving a power of 18 watts when a lamp is connected at 2.1 m of the transmitter ring system [11]. The system has an efficiency of 14.43% at 10 mm of distance.

A method of wireless power transfer technique is called Strongly Coupled Magnetic Resonance (SCMR) which take the advantage of electromagnetic resonance to efficiently transfer power over mid-range distances. A novel approach is the use of a wideband SCMR to mitigate the drop of efficiency caused by the shift of the resonance frequency [12]. However, most of the research in SCMR is at the simulation stage with a limited number of experimental results [13]. Although with these devices great range in the transmission of electric energy is achieved, they are macroscopic devices and are not viable, for example, to be used to charge mobile devices.

In this work, a magnetic resonant coupling system using high frequency energy is presented. The system was designed to increase the signal range by reducing the receiver energy losses and use commercial electronic components to reduce the size of the circuit and allow its implementation in a mobile device. Resonant circuits applied to the transmission and reception of wireless electrical energy are analyzed theoretically and experimentally. The implemented circuit has the advantage of use commercial components that can be implemented in a printed circuit board in SMT package. Figure 1 shows the scheme of wireless power transfer system with magnetic coupling.
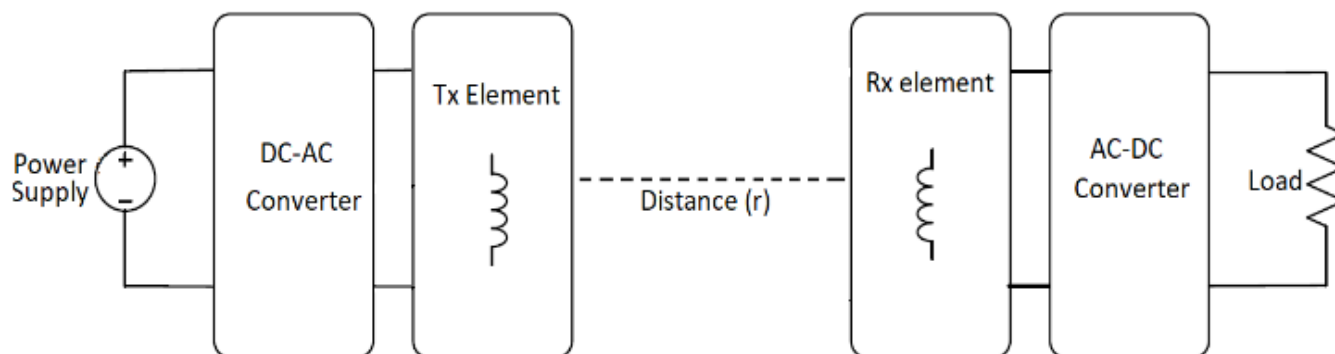

Figure 1. Scheme of wireless power transfer with magnetic coupling.

This article is structured as follows. In section 2, the resonant solid-state device is presented. In section 3, the design of an electromagnetic wave receiver is shown. In section 4, a relationship of the voltage received by the receiver and the transmitting range of the emitter is presented. In section 5, an analysis of the current is presented and, finally, the conclusions are shown in section 6.
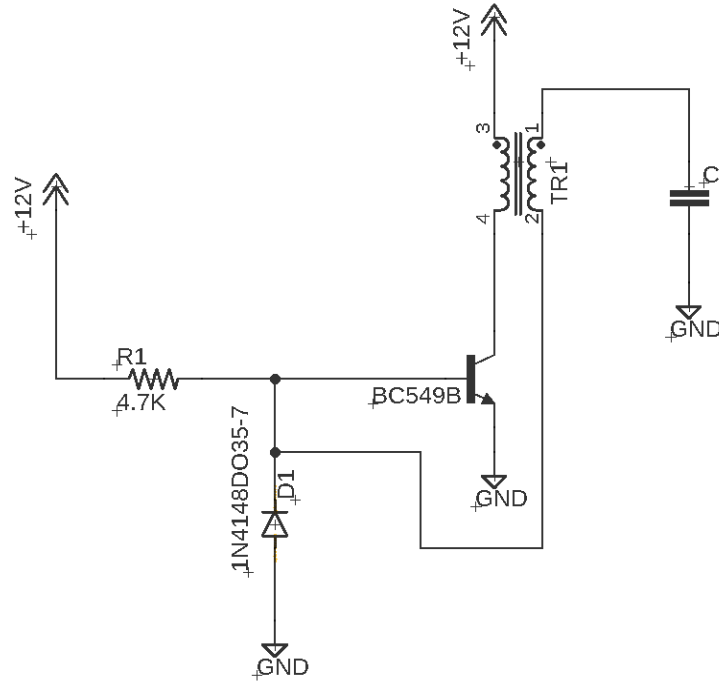
2. Resonant solid state device

2.1. Primary winding analysis

In this section, a resonant solid-state device is analyzed. Some results and simulations corresponding to its operation are presented. Figure 2 shows a schematic diagram of the device. Its operation is based on the transistor, in switch configuration, working as a high frequency function generator, which transforms the primary winding (PW) and secondary winding (SW) in an RLC circuit, with a resonance frequency tuned to the corresponding transistor resonance.

The circuit of Figure 2 is a resonant circuit. When the circuit is powered up, current flow to the base terminal of the transistor through R1. In this condition the transistor is activated and the current start to flow to the PW, producing a magnetic flux which causes a high voltage in the SW since it has more turns than the PW. As the current in the PW increases, the transistor gets into saturated region and due to both the PW and R1 are connected to the +12V, all the current flow through PW causing a current drop through R1 and this condition turn off the transistor. The current start to flow again to the base terminal of the transistor and this cycle is repeated.

The SW, as well as the PW, when a high-frequency signal is applied, shows a parasitic capacitance. Due to the geometry of the winding, the PW and SW have a parasitic capacitance C_1 and C_2 respectively.

**Figure 2.** Resonant solid-state device.

The coil on the left side of the device corresponds to the PW, with a winding length $l = 0.556$ m. The height h of the primary winding is 6.6×10^{-3} m and the number of turns is 5.

The wire diameter of the winding is 6.438×10^{-4} m. It should be noted that this diameter does not include insulation. With insulation, its diameter is 1.32×10^{-3} m.

The radius r_1 of the PW core is 1.27×10^{-2} m.

On the other hand, the Wheeler formula, provides a way to calculate the inductance in windings with air core and circular geometry [14]. This formula is given by,
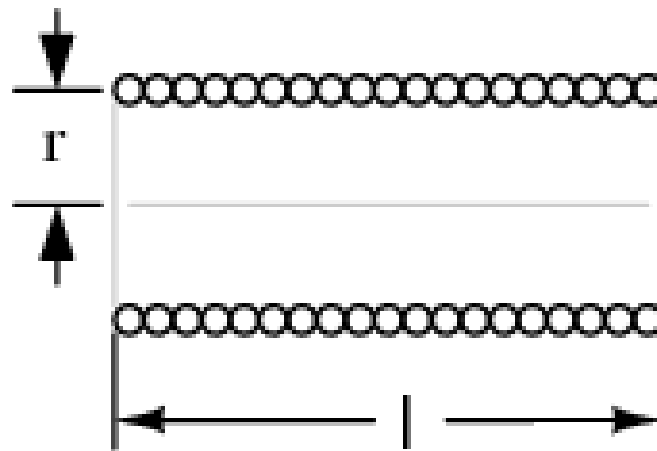
Figure 3. Physical model of a coil

$$L = \frac{0.394 \, r^2 N^2}{9 \, r + 10l}, \qquad (1)$$

where L represents the inductance of the coil, r corresponds to the radius of the coil, l represents the length and N is the number of turns of the winding. These parameters are represented in figure 3.

Using the Wheeler formula, Eq. (1), the inductance L_1 corresponding to the PW is 0.88 μH.

$$Z = \sqrt{R^2 + (X_L - X_C)^2}. \qquad (2)$$

The value minimum of Z, is obtained when $X_L = X_C$.

$$\omega_0 = \frac{1}{\sqrt{LC}}, \qquad (3)$$

where ω_0 corresponds to the resonant frequency in *rad/s,* and $\omega_0 = 2\pi F_0$, resulting the following relation

From the previous results, and through Eq. (4), the resonance frequency F_0 of PW is $3.247 \, MHz$.

The PW shows a resonance by itself, and implicitly presents a capacitance when a high frequency is applied. This parasitic capacitance C_1 corresponds to a value of 2.71 nF.

On the other hand, the impedance Z for our RLC circuit, is defined by,

With $X_L = \omega L$ and $X_C = 1/\omega C$.

By matching the reactances as a function of the frequencies, the following expression results,

$$F_0 = \frac{1}{2\pi\sqrt{LC}} \qquad (4)$$

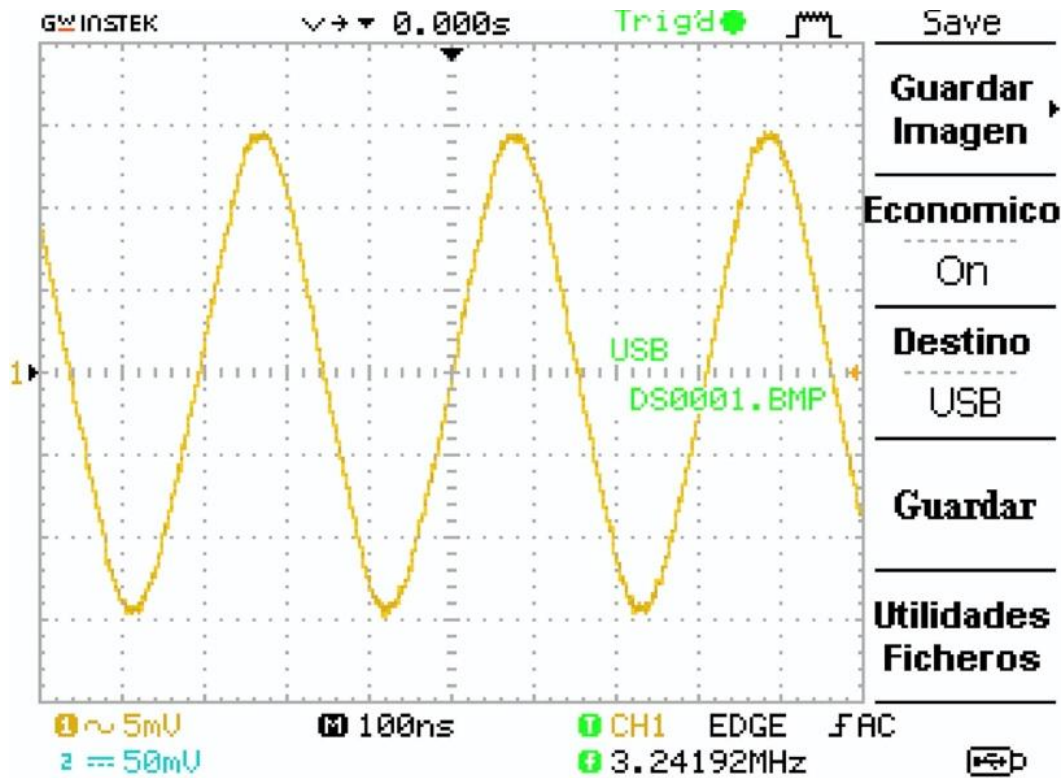This frequency was confirmed by measuring it with an oscilloscope as shown in figure 4.

Figure 4. Measurement of the resonance frequency using an oscilloscope.

2.2 Secondary winding analysis

The winding shown on the right side of the device of Figure 2, corresponds to the SW. This winding has a radius of 1.275×10^{-4} m, a cross section of 5.10×10^{-8} m^2 and a winding length of 18.04 m. Its resistance is 6.0506 Ω, and the height h_2 is, 5.8×10^{-2} m.

On the other hand, the number of turns of the SW is 212. With the previous data and using the Eq. (1), we calculate the inductance L_2 of SW, yielding a value of 411.36 μH.

Through Eq. (4) and using the resonance frequency F_0, as well as the inductance L_2, the calculated parasitic capacitance is 5.8405 pF.

2.3 Potential energy and maximum voltage of secondary winding

The SW has a capacitance at high frequency (parasitic capacitance) and also a capacitance between each turn (intrinsic capacitance). Using the model of a cylindrical solenoid, and the equation of Medhurst [12], which gives a capacitance per unit of length. We can calculate the capacitance C_{L2} for the SW.

$$C_{L2} = \left(0.29\, h_2 + 0.41\, r_2 + 1.94\, \sqrt{\frac{r_2^3}{h_2}} \right) pF/in. \quad (5)$$

Substituting the corresponding values in the previous equation, gives a value of $C_{L2} = 1.32\, pF$.

The total capacitance of the SW can be obtained as the difference of the capacitance C_2 and C_{L2}, which is called C_R or real capacitance. C_{L2} is present even when no current is flowing in SW. The capacitance per unit length without load, is as follow,

$$C_R = C_2 - C_{L2} = 4.52 \ pF. \qquad (6)$$

When a load is placed on the SW, the resulting capacitance per unit of length C_D, can be calculate with the following equation.

$$C_D = 1.4 \left(1.2781 - \frac{D_2}{D_1}\right) \sqrt{\pi \ D_2 (D_1 - D_2)} \ pF/in. \qquad (7)$$

The winding diameters of the core of PW and SW are $D_1 = 1.0 \ in$ and $D_2 = 0.01 \ in$ respectively. Using the Eq (7), C_D is $0.31 \ pF$. When the load is placed on the SW, a discharge occurs on capacitor C_D, and the capacitance decreases, while the voltage increases.

In order to know the maximum voltage on the extreme of the SW, it is necessary to know the stored energy in the winding, so the input voltage in the PW is also required.

The equation that defines the energy with respect to voltage and capacitance, for the PW, is written as follows,

$$E_{PW} = \frac{1}{2} C_1 V_{PW}^2. \qquad (8)$$

Substituting the corresponding values in Eq. (8), the resulting energy in the PW corresponds to $1.91 \times 10^{-7} \ J$. Assuming there is no loss of energy transfer between the PW and the SW, we can say that $E_{PW} = E_{SW}$, where E_{SW} is the energy of the SW.

As the load resistance of cooper makes contact with the tip of the SW, the open circuit voltage V_{OC} increases. To calculate this voltage, we can use the Eq (8) for the SW, resulting,

$$V_{0C} = \sqrt{\frac{2E_{SW}}{C_D}} = 1110.7 \ V. \qquad (9)$$

The real voltage V_{OR} of the SW without load, can be calculated, using the real capacitance C_R, which is equal to 290.7 V.

3. Electromagnetic wave receiver

A good receiver design is crucial to improve the system energy transfer. Figure 4 shows an electromagnetic wave receiver (EMWR), designed to measure the resonance frequency and the voltage V_r, at a distance r from the extreme of the SW, as well as the power in that distance. Also, the EMWR receive the electromagnetic waves emitted by the SW, which go through a process of amplification and decoding, to convert the resulting electric field E_r, into a potential V_r. The EMWR includes a PSoC microcontroller, which is a device with a CPU core and mixed-signal arrays of configurable integrated analog and digital peripherals.

This PSoC microcontroller was configured to acquire the transmitted signal. An analog to digital converter was used to measure the receiver voltage. Also, a comparator was configured to measure the frequency of the signal. An ultrasonic sensor was used to measure automatically the distance between the transmitter and receiver. A display was configured to show the received voltage in SW, the range r and the frequency. The PSoC microcontroller was also configured to send the received information to a PC with Matlab software to save the data in a log file and plot the corresponding curves. Figure 6 shows the diagram of the PSoC microcontroller and the receiver circuit.
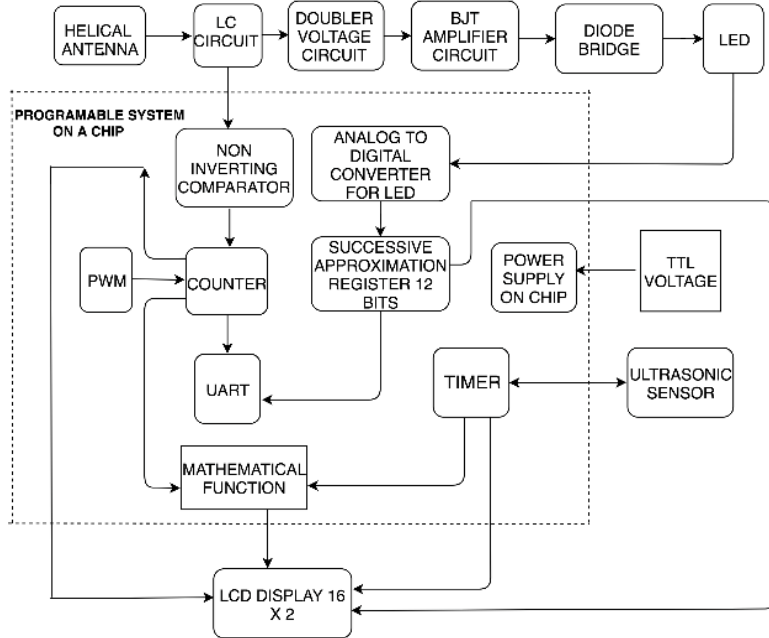
Figure 5. Electromagnetic wave receiver (EMWR).
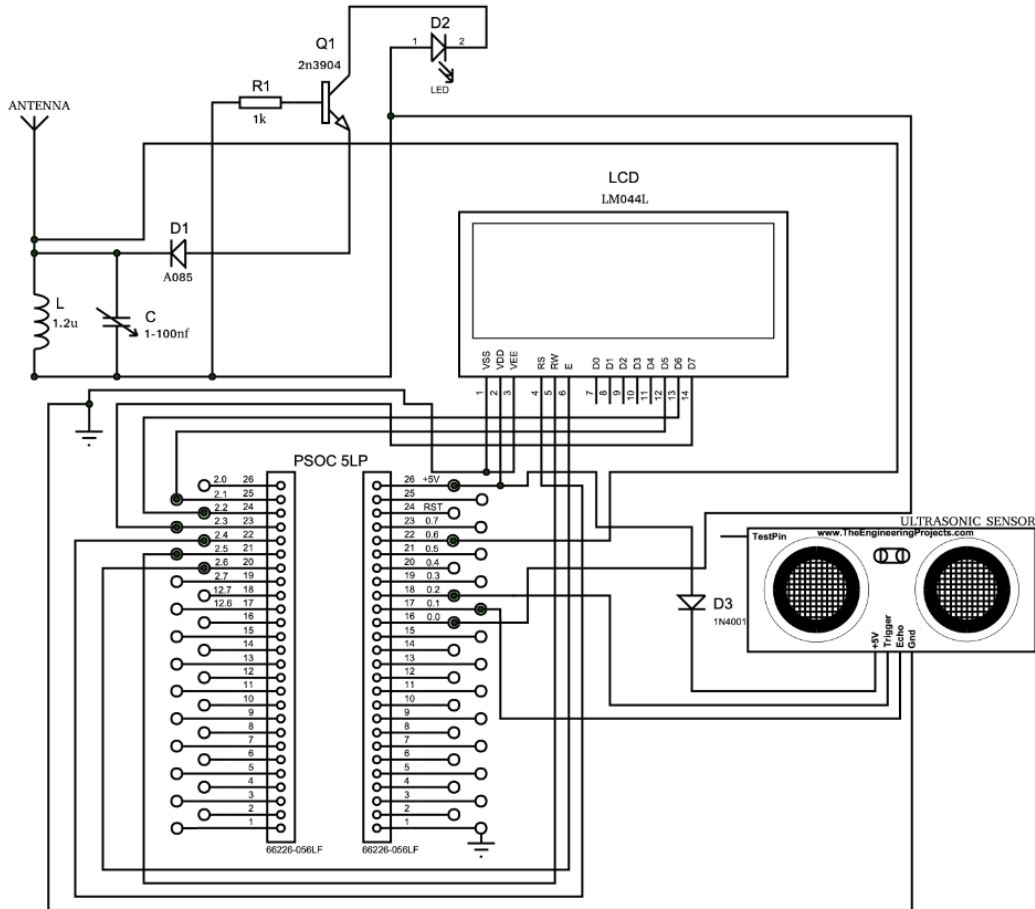

Figure 6. Circuit diagram of the receiver.

4. Secondary winding

In order to perform a quantitative study to know the variation of the voltage corresponding to the SW, as a function of the distance r regard to the detector.

Using the Gauss theorem, expressed as,

$$\oint \boldsymbol{E} \cdot \boldsymbol{ds} = \frac{Q}{\varepsilon_0}. \qquad (10)$$

The cylindrical Gaussian surface is represented in figure 7, where R corresponds to the radius of the SW, and r corresponds to the radius of the Gaussian surface. We can calculate the electric field E, at a distance r from SW.

Let ds be a differential element of surface, where the electric field E and this ds are parallel in the lateral surface, whereas in the upper and lower surfaces, they are perpendicular.
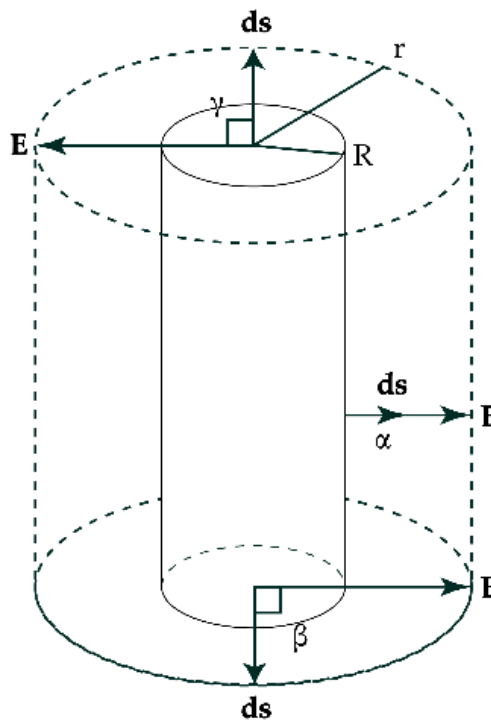

Figure 7. Gaussian surface around the SW.

The angles γ and β in the cylinder caps that form E and ds are perpendicular, while α, corresponding to the angle between E and ds of the lateral surface of the cylinder, is zero degrees.

According to Gauss's theorem, for the lower and upper surface, we find that,

$$\oint E \, ds \cos \beta = \oint E \, ds \cos \gamma = 0. \qquad (11)$$

Therefore, it is shown that the electric field on the upper and lower surface is zero.

On the other hand, for the lateral Gaussian surface

$$\oint \boldsymbol{E} \cdot \boldsymbol{ds} = \oint E \, ds \cos \alpha. \qquad (12)$$

Since the electric field is uniform throughout the lateral periphery of the Gaussian surface,

322

$$E \oint ds = Es, \qquad (13)$$

Where $s = 2\pi rL$, L corresponds to the height of the cylindrical surface, *s,* represents the lateral surface of the cylinder. Thus

$$Es = 2\pi rEL . \qquad (14)$$

From eq. (10) results,

$$2\pi rEL = \frac{Q}{\varepsilon_0}, \qquad (15)$$

where Q is the total charge of the cylinder.

The SW is formed by a winding that contains multiple turns. These capacitors are in parallel, forming a cylindrical capacitor with a total capacitance C, which stores a charge that will be proportional to the voltage in the secondary winding V_{SW}. Using the model to calculate the electric field in a cylindrical capacitor [15].

$$C = \frac{2\pi\varepsilon L}{ln\left(\frac{r}{R}\right)}, \qquad (16)$$

where ε and L, are the permittivity of the insulator and the height the cylinder respectively.

Using the capacitance C in the equation that defines the charge $(Q = CV)$, and the result in eq. (15), the equation that defines the electric field as a function of distance r is,

$$E = \frac{\varepsilon V_{SW}}{\varepsilon_0 rln\left(\frac{r}{R}\right)}, \qquad (17)$$

where ε_0 is the electric permittivity in vacuum,

On the other hand, to obtain an expression for V_2, which is the voltage measured by the electromagnetic wave receiver (EMWR), as a function of the distance r, we use the knowledge the electric field E, is expressed as the voltage V divided by the distance r. In our case, r expresses the electric field reaching E in terms of voltage V_2, processed by the receiver placed at the distance r of the SW. From the above, and the Eq. (17), the voltage V_2 can be expressed as,

$$V_2 = \frac{\varepsilon V_{SW}}{\varepsilon_0 ln\left(\frac{r}{R}\right)}. \qquad (18)$$

From Eq. (18) we can obtain an expression to calculate the reaching r as a function of the transmitting voltage V_{SW} and the receiving voltage V_2.

$$r = Re^{\frac{\sigma V_{SW}}{V_2}}, \qquad (19)$$

where $\sigma = \varepsilon/\varepsilon_0$.

The figure 8, is a block diagram that represents the SW voltage and EMWR.
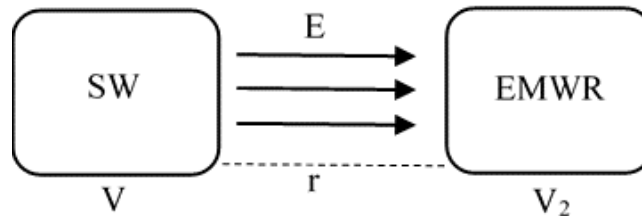

Figure 8. Block diagram of SW and EMWR

To increase the reaching range r, it is necessary to increase the radius R of the ES, as well the as the electrical permittivity in the insulator and the number of windings. The Eq. (19) provides us with a nice relation of the relevant parameters of the system to obtain a greater range r of voltage

323

V_2. And corresponds to a one of the principal results of this paper.

From Eq. (19) we note that if the voltage V_2 tends to 0, then r tends to infinity as is shown in Fig. 8. On the other hand, if V_2 tends to infinity, r tends to R, which is an expected result, since the

maximum voltage V_2 occurs at the minimum distance, when $r = R$.

It is important to highlight that all the parameters of Eq. (18) can be measured, and gives the effective voltage drop V$_2$, as a function of distance r.
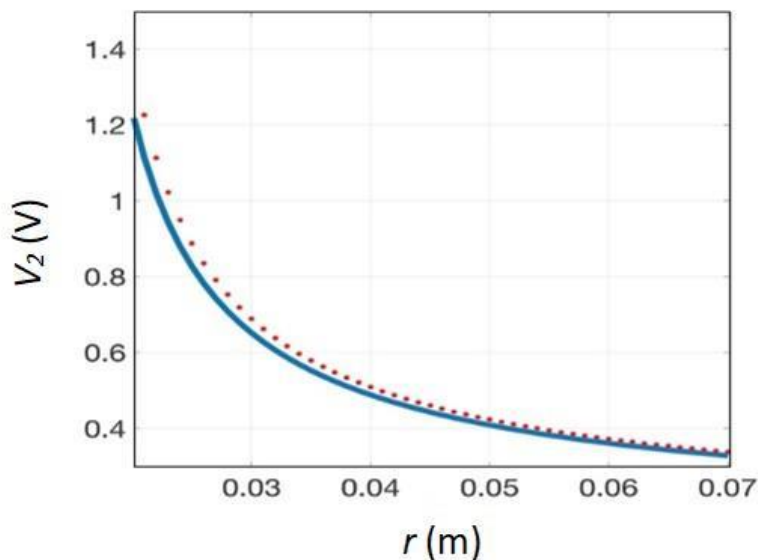
Figure 9. Voltage V$_2$ as function of the range r. The red dotted line corresponds to experimental data. The blue continuous line is obtained theoretically from Eq. (14).

In figure 9, the experimental voltage was obtained in a real-time interface that communicates a PSoC microcontroller and a Matlab script. We can see both experimental and theorical (Eq. (18)) curves show the same behavior.
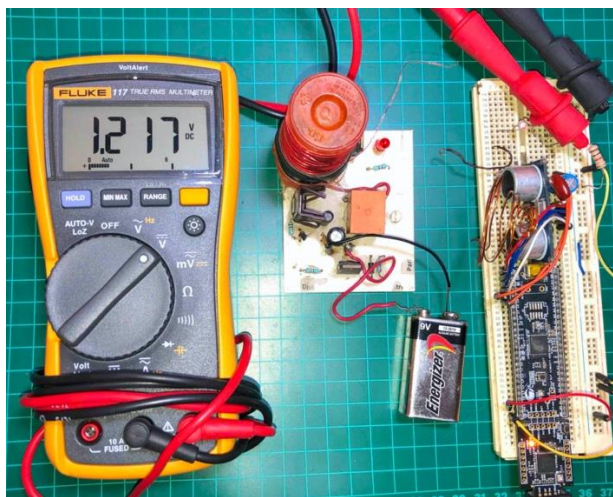
Figure 10. From left to right, is shown multimeter, SW and EMWR

In figure 10, is observed that the maximum voltage measured in the EMWR is 1.217 V. This is close to theoretical value given by Eq. (18).

5. Electrical current analysis

Knowing that the resonance frequency F_0 of the ES, corresponds to 3.25 MHz, the coil and capacitor of the EMWR are 411.3 µH and 5.8 pF respectively, and that these form a resonant LC circuit, we can obtain the current in the LC circuit.

In resonance, it can be calculated the parameters of a free LC oscillator, without using a power supply, using the simple equation,

$$L\frac{di}{dt} + \frac{Q}{C} = 0. \qquad (20)$$

It is found that the charge on the capacitor is,

$$Q = Q_{max} \cos\frac{t}{\sqrt{LC}}. \qquad (21)$$

While the current in the LC oscillator corresponds to,

$$i = -\frac{1}{\sqrt{LC}} Q_{max} \sin\frac{t}{\sqrt{LC}}. \qquad (22)$$

In this way, the amplitude of the maximum current of the LC circuit it is obtained,

$$i_{LC} = \frac{1}{\sqrt{LC}} Q_{max}. \qquad (23)$$

We know that the capacitance is given by the reason of the charge and the voltage, the current of the LC circuit as function of the ES voltage is obtained, replacing L and C by L_{EMWR} and C_{EMWR}, i_{LC} leads to,

$$i_{LC} = \frac{C_{EMWR}V_2}{\sqrt{L_{EMWR}C_{EMWR}}}. \qquad (24)$$

Substituting the values of C_{EMWR}, V_2 and L_{EMWR}, in the previous equation, we obtain the value of $i_{LC} = 158$ µA, which is the maximum rms current that goes through L_{EMWR} or C_{EMWR}. To enhance the current in the EMWR, is necessary to increase V_2 and C_{EMWR}, nevertheless, by varying C_{EMWR}, the ES will no longer be in resonance with the EMWR, unless in both systems increase the capacitance proportionally.

In figure 11, the measured current i_{LC} is plotted as function of the range *r*. We can see a maximum initial value of 149 µA, which is near than the calculated value.
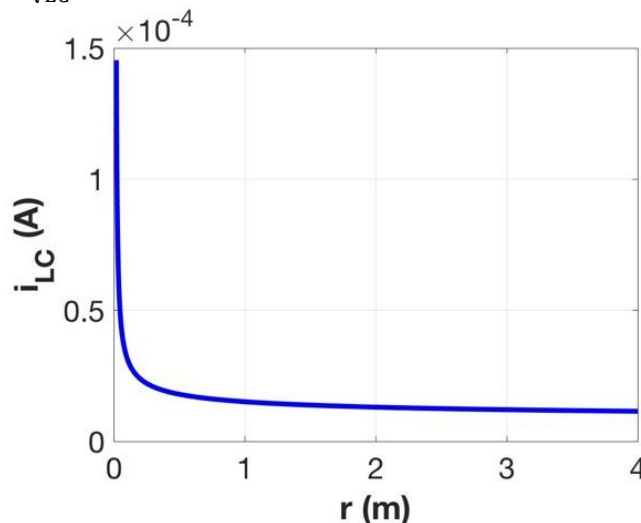

Figure 11. Total current passing through the coil and the capacitor of the electromagnetic wave receiver

325

Unlike the measurement presented in figure 10, the current measurement is carried out using a high resolution miltimeter, this because the current received by the EMWR is in the order of micro-Ampere. If you want to measurement the

current with a low-resolution multimeter you will not be able measure it. The measuring instrument used was the Fluke 87. The measurement is shown in figure 11.
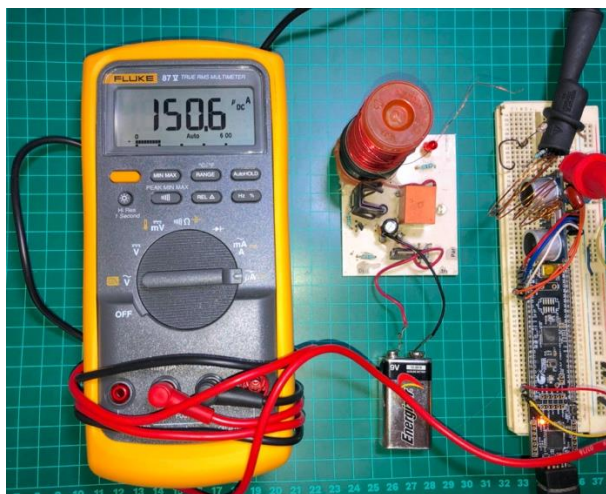
Figure 11. Measurement of current in the EMWR.

The value of 150.06 μA is close to the theoretical result obtained in the Eq. (24).

6. Conclusions

In this work, a theoretical framework was implemented to analyze a solid-state resonant circuit, based on a designed device for transmitting and receiving wireless electrical energy. Both, theoretical and experimental results were obtained for the energy transmission and reception of energy. Also, analytical expression was obtained to calculate the effective voltage as a function of the distance from the secondary coil to the receiver. This expression allows us to explore the parameter necessary to achieve a greater range V_2.

Using the PSoC microcontroller coupled to the electromagnetic waves receiver to acquire the received voltage and distance. A visual interface was designed in real time to plot the behavior of

the effective voltage that the SW emits, with respect to the distance of the receiver, observing a concordance between the theoretical and experimental value. It was demonstrated, that the voltage at the receiver, decreases exponentially as function of the range.

The current in the front end of the electromagnetic wave receiver was calculated, it also shows an exponential decay as a function of the range.

We obtained that for increase the range, it is necessary to increase the radius R, as well as the electrical permittivity in the insulator and the number of windings, by varying both parameters, it is observed experimentally that the range increases exponentially.

It was shown that the resonance frequency of the secondary winding is constant, regardless of a load.

References

The advantage of our results compared to others reported in the, is that although exist devices great range in the transmission of electric energy is achieved, they are macroscopic devices and are not viable, for example, to be used to charge mobile devices.

While the system presented here was designed to increase the signal range by reducing the receiver energy losses and use commercial electronic components to reduce the size of the circuit and allow its implementation in a mobile device, as is the case of the device shown here, which is small in size and can be used in recharging this purpose.

7. Acknowledgments

8. Authorship acknowledgment

Sergo Orendain castro: Conceptualización; Recursos; Ideas; Metodología; Análisis formal; Investigación; Recursos; Análisis de datos; Borrador original. *Eduardo Murillo Bracamontes:* Conceptualización; Ideas; Investigación; Análisis de datos; Escritura. *Oscar Edel Contreras López:* Adquisición de fondos y Administración de proyecto. *Alberto Hernández Maldonado:* Conceptualización; Ideas; Metodología; Análisis formal; Investigación; Análisis de datos; Escritura; Borrador original; Revisión y edición; Administración de proyecto.

[1] X. Lu, P. Wang, D. Niyato, D. I. Kim, and Z. Han, "Wireless Charging Technologies: Fundamentals, Standards, and Network Applications," IEEE Commun. Surv. Tutorials, vol. 18, no. 2, pp. 1413-1452, 2016. https://doi.org/10.1109/COMST.2015.2499783.

[2] K. H. Yi, "Output voltage analysis of inductive wireless power transfer with series lc and llc resonance operations depending on coupling condition," Electron., vol. 9, no. 4, 2020. https://doi.org/10.3390/electronics9040592.

[3] P.S. Riehl et al., "Wireless power systems for mobile devices supporting inductive and resonant operating modes," IEEE Trans. Microw. Theory Tech., vol. 63, no. 3, pp. 780-790, 2015. https://doi.org/10.1109/TMTT.2015.2398413.

[4] N. Tesla, "Experiments with altrnate current of very high frequency and their application to methods of artificial illumination," Columbia Coll., pp. 267-319, 1891. https://doi.org/10.1109/T-AIEE.1891.5570149.

[5] S. K. Oruganti and F. Bien, "Investigation of Near-Field Wireless Energy Transfer for Through Metal-Wall Applications," 2014 IEEE Wirel. Power Transf. Conf., pp. 247-250, 2014. https://doi.org/10.1109/WPT.2014.6839573

[6] S. Kim, Y. Lim, and S. Lee, "Magnetic Resonant Coupling Based Wireless Power Transfer System with In-Band Communication," no. May 2015, 2013. https://doi.org/10.5573/JSTS.2013.13.6.562

[7] R. Kerid and H. Bourouina, "Analysis of Wireless Power Transfer System with New Resonant Circuit for High Efficiency Using Perforated Capacitors," Arab. J. Sci. Eng., vol.

44, no. 3, pp. 2445-2451, 2019. https://doi.org/10.1007/s13369-018-3579-2.

[8] P. Sittithai, K. Phaebua, T. Lertwiriyaprapa, and P. Akkaraekthalin, "Magnetic field shaping technique for HF-RFID and NFC systems," Radioengineering, vol. 27, no. 1, pp. 121-128, 2019. https://doi.org/10.13164/re.2019.0121

[9] R. A. Moffatt, "Wireless Transfer of Electric Power," Massachusetts Institute of Technology, 2009.

[10] T. Supriyanto, A. Wulandari, and T. Firmansyah, "Design and Comparison Wireless Power Transfer Base on Copper (Cu) and Aluminium (Al) Rings Loop Magnetic Coupling," no. January 2016, pp. 6-10, 2017. https://doi.org/10.18178/IJIEE.2016.6.2.605

[11] C. K. Lee, W. X. Zhong, and S. Y. R. Hui, "Effects of Magnetic Coupling of Nonadjacent Resonators on Wireless Power Domino-Resonator Systems," vol. 27, no. 4, pp. 1905-1916, 2012. https://doi.org/10.1109/TPEL.2011.2169460

[12] W. Zhou, S. Sandeep, P. Wu, P. Yang, W. Yu, and S. Y. Huang, "A wideband strongly coupled magnetic resonance wireless power transfer system and its circuit analysis," IEEE Microw. Wirel. Components Lett., vol. 28, no. 12, pp. 1152-1154, 2018. https://doi.org/10.1109/LMWC.2018.2876767

[13] C. M. W. Basnayaka, D. N. K. Jayakody, A. Sharma, H.-C. Wang, and P. Muthuchidambaranathan, "Performance Study of Strongly Coupled Magnetic Resonance," 2019, [Online]. Available: http://arxiv.org/abs/1908.02541.

[14] D. Knight, The self-resonance and self-capacitance of solenoid coils: applicable theory, models and calculation methods, no. May. 2016.

[15] P. Azimi and H. Golnabi, "Precise Formulation of Electrical capacitance for a Cylindrical Capacitive Sensor," J. Appl. Sci., vol. 9, no. 8, pp. 1556-1561, 2009. https://doi.org/10.3923/jas.2009.1556.1561

[16] H. Wheeler, "Formulas the Skin Effect," Proc. IRE, pp. 412-424, 1942. https://doi.org/10.1109/JRPROC.1942.232015